# Indonesian Physical Review

Volume 9 Issue 02, May 2026
P-ISSN: 2615-1278, E-ISSN: 2614-7904

# Study of Ekman Mass Transport and Ekman Pumping Velocity in the Southern Waters of Java – Nusa Tenggara from 2003 to 2024

**Nindy Saitama L. Gaol[1], I Wayan Gede Astawa Karang[1,2*], I Dewa Nyoman Nurweda Putra[1]**
[1] *Department of Marine Sciences, Faculty of Marine Science and Fisheries, Udayana University, Bali, Indonesia*
[2] *Center for Remote Sensing and Ocean Sciences (CReSOS), Udayana University, Bali, Indonesia*

*Corresponding Author's E-mail: gedekarang@unud.ac.id*

**Article Info**

***Article info:***
*Received: 29-08-2025*
*Revised: 31-12-2025*
*Accepted: 18-01-2026*

***Keywords:***
*EMT; EPV; SST; Chlorophyll-a; ENSO; IOD.*

***How To Cite:***
*N. S. L. Gaol, I. W. G. A. Karang, I. D. N. N. Putra, "Study of Ekman Mass Transport and Ekman Pumping Velocity in the Southern Waters of Java – Nusa Tenggara from 2003 to 2024", Indonesian Physical Review, vol. 9, no. 2, p 202-226, 2026.*

***DOI:***
*https://doi.org/10.29303/ipr.v9i2.565.*

**Abstract**

*The waters south of Java to Nusa Tenggara are a critical upwelling region heavily influenced by monsoon dynamics. The interactions drive oceanographic variability, specifically Ekman Mass Transport (EMT) and Ekman Pumping Velocity (EPV), which regulate primary productivity. While previous studies have examined these dynamics, most have focused on short-term variations. To address this, this study analyzes the variability of EMT and EPV over a 22-year period (2003–2024) and their interaction with El Niño-Southern Oscillation (ENSO) and Indian Ocean Dipole (IOD). EMT and EPV values were calculated using ECMWF wind data, SST, and chlorophyll-a data sourced from MODIS, and climate indices (Niño 3.4 and DMI), which were then analyzed using Pearson correlation. Results show that EMT and EPV peak during the Southeast Monsoon (JJA), reaching approximately 5.16 $m^2/s$ and -2.89 × $10^{-5}$ m/s, respectively. Notable anomalies occurred in 2010 and 2016; specifically, the 2010 interaction between La Niña and a negative IOD significantly suppressed upwelling. Correlation analysis reveals that SST is predominantly influenced by EPV, while chlorophyll a concentration is more closely linked to EMT. Although both ENSO and IOD modulate these dynamics, the IOD exerts a stronger influence due to the region's proximity to the Indian Ocean. These findings provide critical insights into the oceanographic drivers of regional productivity, supporting sustainable fisheries management.*



## Introduction

The movement of ocean currents can encourage upwelling and downwelling through wind-driven Ekman dynamics, which consist of Ekman Mass Transport (EMT) and Ekman Pumping Velocity (EPV) [1], [2]. EMT is a wind-driven process along the coast that pushes surface water away from the shoreline, causing surface water to sink or bringing deeper water to the surface layer by balancing mass loss near the coast [3]. EPV is the movement of water mass toward the seabed (downwelling) or the vertical movement of water mass toward the surface (upwelling), depending on convergence and divergence at the sea surface [2]. Upwelling can cause sea

surface temperatures (SSTs) to be low and chlorophyll a concentration to be high, thereby enhancing water productivity and positively impacting the economy [4]. Conversely, low chlorophyll a concentration and rising SST are referred to as the downwelling process [5].

In Indonesian waters, upwelling occurs in several regions, one of which is from southern Java to southern Nusa Tenggara, which falls under the Indonesian Fisheries Management Area (WPP-RI) 573 [6]. This study area is of interest because it is influenced by oceanographic-atmospheric phenomena. El Niño Southern Oscillation (ENSO) and the Indian Oscillation Dipole mode (IOD) are oceanographic phenomena that affect the waters, which is the outflow path of the Indonesian Throughflow (ITF) [7]. These waters are highly dynamic, with wind strength and direction changing seasonally based on the northwest and southeast monsoon seasons, which can cause EMT and EPV [8], [4].

Studies on the variability of EMT and EPV in relation to SST and chlorophyll a, as well as the effects of IOD and ENSO on EMT and EPV, have previously been conducted along the waters south of Java [2]. The occurrence of EMT and EPV causes upwelling with parameters of SST and chlorophyll a in the waters south of Java–Sumbawa has also been studied by [4]. Additionally, research on SST dynamics, chlorophyll a, and wind in the waters of Southern Java–Nusa Tenggara and their relationship with ENSO and IOD from 2003 to 2023 has been conducted by [9]. However, studies on EMT and EPV in the southern waters of Java–Nusa Tenggara from 2003 to 2024 have not been examined in previous research. This study also examines the influence of EMT and EPV on SST and chlorophyll a, as well as the influence of ENSO and IOD on EMT and EPV. This study was conducted to analyze the variability of EMT and EPV, the influence of EMT and EPV on SST and chlorophyll a, and the influence of ENSO and IOD on EMT and EPV. The findings of this study are expected to contribute to understanding oceanographic dynamics in the study area and to support more sustainable fisheries resource management.

## Research Area

The research area was in the southern waters of Java and Nusa Tenggara, with coordinates 6° S - 13° S and 105° E - 129° E, from January 2003 to December 2024 (22 years). Furthermore, plots were made across several regions to analyze local characteristics, given the study area's diversity. The area was divide into four regions: Region A covers Southwest Java (7.5° S – 8.5° S, 105.25° E – 107.5° E), Region B covering Southeast Java (8.5° S – 9.5° S, 112° E – 114.5°), Region C covers South Bali (8.5° S – 9.5° S, 114.5° E – 116°), and Region D covers the Sawu Sea (9.5° S – 10.5° S, 121.25° E – 123.25° E) as shown on the research map (Figure 1).

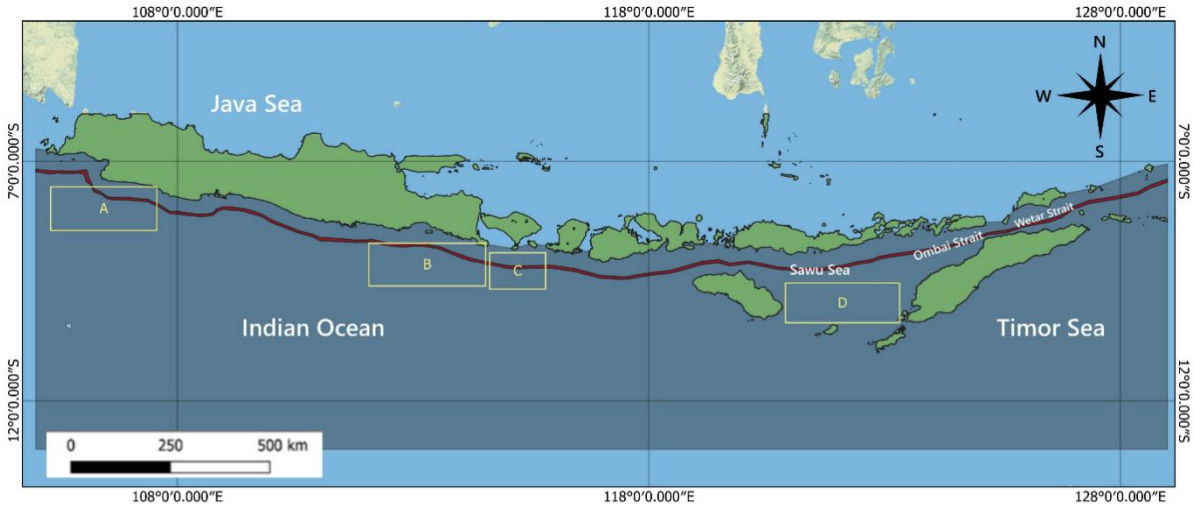


**Figure 1.** Study area, extraction area (Red Polygon) for Hovmöller Diagram, and plot area for correlation; region A is Southwest Java, region B is Southeast Java, region C is South Bali, and region D is Sawu Sea.

## Data and Methods

Wind data uses the Climate Data Store (https://cds.climate.copernicus.eu/) from the European Centre for Medium-Range Weather Forecasts (ECMWF) ERA5, which estimates wind speed and direction above sea level at about 10 m, with *u*- and v-components. Chlorophyll-a and SST from the Moderate Resolution Imaging Spectroradiometer (MODIS), because they tend to have little cloud cover [10]. The climate indices used are ENSO and IOD, with climate index data from the 3.4 Anomaly (https://www.cpc.ncep.noaa.gov/data/indices/) and the Dipole Mode Index (DMI) from the same website. The Anomaly 3.4 data were used to identify ENSO and DMI, and to identify IOD. Based on the research by [11], the classification of anomalies is as follows (Table 1).

**Table 1.** Anomaly Index

| Phenomenon | Anomaly Index | Phenomenon | Anomaly Index |
|---|---|---|---|
| Weak El Niño | 0.5°C to 0.99°C | Weak La Niña | -0.5°C to -0.99°C |
| Moderate El Niño | 1.0°C to 1.49°C | Moderate La Niña | -1.0°C to -1.49°C |
| Strong El Niño | 1.5°C to 1.99°C | Strong La Niña | -1.5°C to -1.99°C |
| Very Strong El Niño | >2.0°C | Very Strong La Niña | >-2.0°C |
| Positive IOD | >0.35°C | Negative IOD | <-0.35°C |

## Ekman Mass Transport Calculation

EMT calculations are based on wind stress, assuming that the x-axis wind component is parallel to the coastline and the y-axis wind component is perpendicular to the coastline. According to [12], wind stress can be calculated using the following equation:

$$\tau x = \rho_a \, C_d |\overrightarrow{v_H}| U_{10} \quad (1)$$

$$\tau y = \rho_a \, C_d |\overrightarrow{v_H}| V_{10} \quad (2)$$

In addition, the Coriolis parameter calculation can use the following formula [13]

$$f = 2\,\Omega \sin\varphi \tag{3}$$

EMT ($m^2/s$) calculations use the following equation [13]

$$EMT_X = \frac{\tau y}{\rho_w f} \tag{4}$$

$$EMT_y = -\frac{\tau x}{\rho_w f} \tag{5}$$

where $\tau x, \tau y$ are wind stress vectors (Pa), $C_d$ is the drag coefficient ($1.5 \times 10^{-3}$), $\rho_a$ is air density (1.25 kg/m$^3$), $\overrightarrow{v_H}$ is wind strength (m/s), $U_{10}, V_{10}$ is zonal and meridional wind speeds 10 meters above sea level (m/s), Ω is Earth's rotation rate ($7.29 \times 10^{-5}$ rad/s), Φ is latitude, $\rho_w$ is the density of seawater (1.025 kg/m$^3$), and $f$ is the Coriolis parameter ($s^{-1}$).

## Ekman Pumping Velocity Calculation

EPV calculations are based on wind stress curl, assuming that the x-axis wind component is parallel to the coastline and the y-axis wind component is perpendicular to the coastline. EPV is calculated following the method used by [14] as follows:

$$EPV = -\frac{curl}{\rho_w f} \tag{6}$$

$$curl = \frac{\partial \tau_y}{\partial_x} - \frac{\partial \tau_x}{\partial_y} \tag{7}$$

where curl is the wind stress curl vector (Pa/m), τx, τy are the wind stress vectors (Pa), $\rho_w$ is the density of seawater (1.025 kg/m$^3$), and f the Coriolis parameter ($s^{-1}$).

## Sea Surface Temperature Anomalies and Chlorophyll-a Anomalies Calculation

Deviations in SST and chlorophyll-a values are determined by calculating SST anomalies and chlorophyll-a anomalies. According to [15], calculations of SST and chlorophyll-a data anomalies use the following equations:

$$\text{Anomaly of the i-th month variable} = x_i - X \tag{8}$$

where $x_i$ is monthly data and $X$ is the monthly average value.

## Correlation Analysis

Pearson's correlation analysis method is used to assess the effects of EMT and EPV on SST and Chlorophyll-a, as well as the impact of ENSO and IOD on EMT and EPV. Data from SST, chlorophyll-a concentration, and wind must have the same number of data points/pixels or the same data matrix size to enable correlation analysis between SST and chlorophyll-a variables using EMT and EPV. Based on the research by [16], matrices that are not the same are adjusted to reduce data dimensions and detect the most dominant patterns and structures. Therefore, SST and chlorophyll-a data with a spatial resolution of 4 km were adjusted to wind data with a spatial resolution of 25 km by aggregating (mean aggregation) smaller units (pixels) into larger units. Mean aggregation is the process of taking the average value of small grids to produce larger grids [17]. According to research by [18], correlation can be calculated using the formula:

$$r = \frac{N\,(\Sigma\,XY) - (\Sigma x \Sigma y)}{\sqrt{N\,\Sigma x^2 - (\Sigma X)^2 (\mathrm{N}\,\Sigma y^2 - (\Sigma y)^2)}} \quad (9)$$

where r is the coefficient of correlation, X is the independent variable (control variable), Y is the dependent variable (controlled variable), and N is the number of data points. The correlation strength values according to [19] are as follows (Table 2):

**Table 2**. Correlation Coefficient

| Level of Correlation | Value Range | Level of Correlation | Value Range |
|---|---|---|---|
| Very Weak Positive | 0 to 0.19 | Very Weak Negative | -0.19 to -0.01 |
| Weak Positive | 0.2 to 0.39 | Weak Negative | -0.39 to -0.2 |
| Moderate Positive | 0.4 to 0.59 | Moderate Negative | -0.59 to -0.4 |
| Strong Positive | 0.6 to 0.79 | Strong Negative | -0.79 to -0.6 |
| Very Strong Positive | 0.8 to 1 | Very Strong Negative | -1 to -0.8 |

## Variability Analysis

Variability analysis was processed to produce monthly climatological composites from 2003 to 2024. The analysis was also conducted based on four seasons, which consist of Northwest Monsoon (DJF), transition season I (MAM), Southeast Monsoon (JJA), and transition season II (SON) [20]. The selection of the four-season analysis was made because it can affect oceanographic conditions, whereas the wind system causes the EMT and EPV patterns to be highly determined by the season [46]. The analysis of SST anomaly trends and chlorophyll-a anomalies used annual averages to produce interannual variations in the waters south of Java until Nusa Tenggara [15]. Furthermore, the analysis of EMT, EPV, SST, and chlorophyll a anomaly used Hovmöller diagrams to characterize the anomalies. A Hovmöller diagram is depicts the temporal and spatial variations of the EMT and EPV processed. The x-axis indicates longitude, and the y-axis indicates time [46]. This diagram uses the extraction area in Figure 1, where pixels are spaced 50 kilometers from the coastline. This aligns with the research by [21] and [9], who conducted analyses approximately 50 km away. Additionally, coastal waters are a restricted zone due to several factors from the land, such as suspended sediments and land turbidity [22], [23]. This can affect the amount of sunlight entering the water, the water's fertility, and phytoplankton growth [47].

## Result and Discussion

### Variability Ekman Mass Transport

Figure 2 shows a monthly distribution map of EMT, with blue to red colors indicating EMT strength from weak (blue) to strong (red) and arrow vectors indicating the direction of movement toward onshore or offshore. The map shows that from December to March, EMT moves toward onshore, while from April to November, it moves toward offshore. Similar findings were also reported by [2], [4]. The occurrence of onshore EMT is due to the Northwest Monsoon being deflected 45° to the left in the southern hemisphere [24], while offshore-directed EMT dominates EMT changes for 8 months, resulting in upwelling in the onshore area [14]. The EMT value reaches its maximum in August at 6.47 $m^2/s$.

Monthly EMT variability is strongly influenced by seasonal changes. EMT has an alternating pattern, especially during the Northwest and Southeast Monsoon in this study area. Figure 3

shows the Northwest Monsoon (DJF), depicting weak EMT intensity with an average of 1.11 m²/s and directed onshore. This aligns with the research by [25] along Central Java, where winds blow from the west during the Northwest monsoon, causing downwelling. During the transition season, I (MAM) observed that the EMT began to shift toward offshore, with very low values averaging 0.65 m²/s. During the Southeast Monsoon (JJA), EMT values vary across regions. In Southwest Java, values reach 5.16 m²/s, while in Central Java and parts of East Nusa Tenggara, values are lower, averaging 2.52 m²/s; in the eastern regions, values reach 4.57 m²/s. The EMT in the Sawu Sea and Ombai Strait is very low compared to other regions, reaching 0.05 m²/s. This is likely due to the South Java Counter Current (SJCC) crossing the Sawu Sea to reach the Ombai Strait, so that the Ekman flow by the Southeast Monsoon has a downward flow in the eastern surface in the northern part of the Ombai Strait [26]. EMT during the Southeast Monsoon season indicates that water masses move away from the coast more strongly than in other seasons, as it is closely related to the Southeast monsoon winds moving from Australia toward Asia and counterclockwise in the southern hemisphere, which results in upwelling [25]. Strong offshore EMT can cause upwelling by lifting low temperature water from the subsurface to the sea surface, leading to higher chlorophyll-a concentrations and reduced SST [14]. During transition season, I (SON), the EMT begins to weaken but remains relatively strong in the western region with values around 4.03 m²/s. According to [3], this occurs because wind stress begins to decrease during the second transitional season.

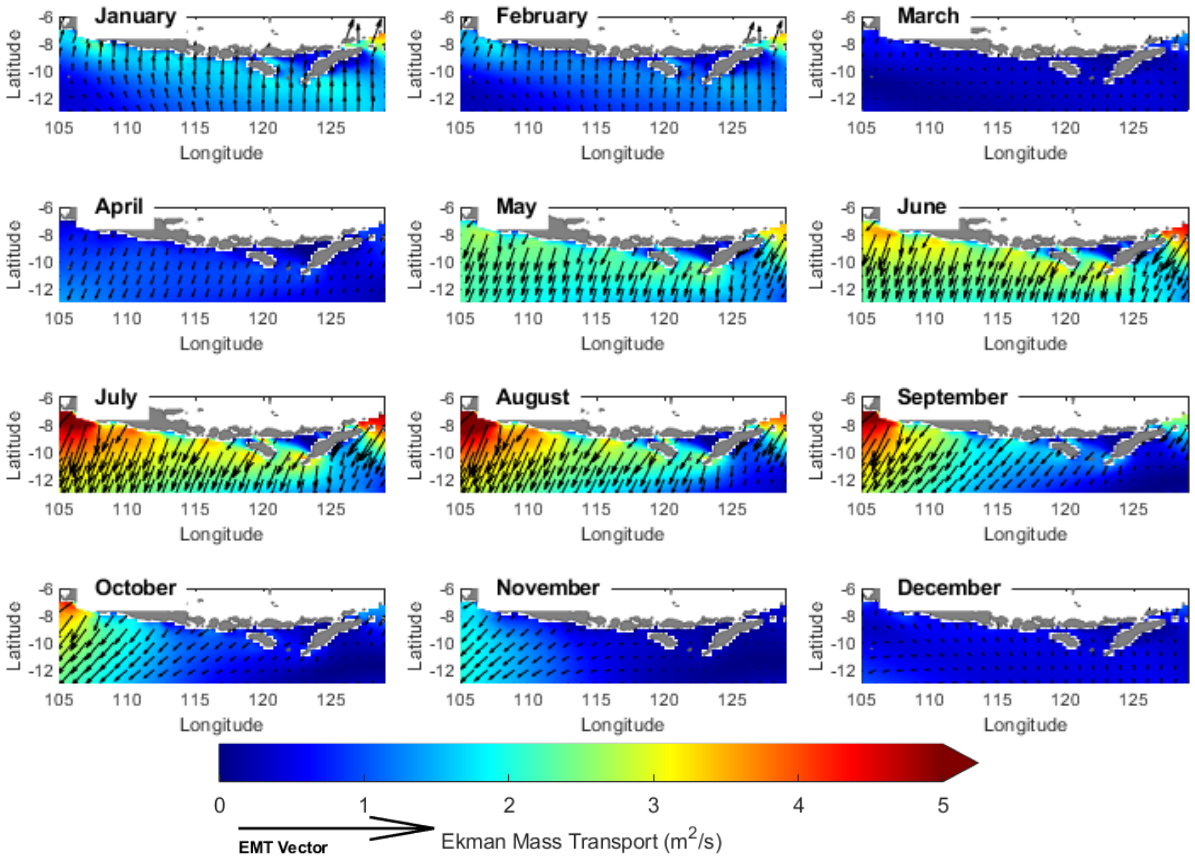


**Figure 2**. The monthly EMT distribution map with shades of blue to red represents changes in EMT strength, with blue indicating relatively weak EMT and red indicating increasingly strong EMT values, while arrows indicate the direction of EMT.

The EMT intensity pattern shows a gradual increase from May to September, followed by very low values in the months that follow.

Seasonal patterns in EMT indicate the role of seasonal cycles in EMT variability, with the highest values occurring in the Southeast monsoon (JJA).

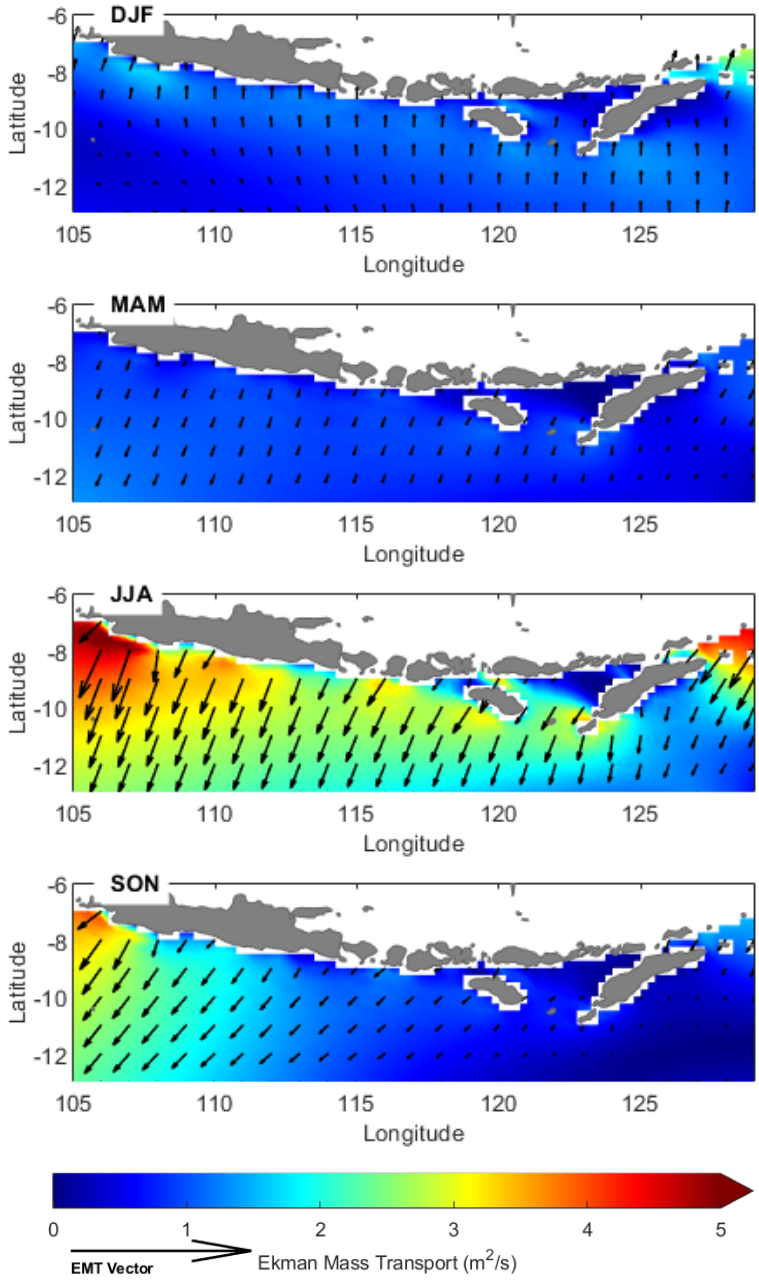


**Figure 3.** Seasonal variability of EMT, the color shading represents the resultant EMT intensity, while arrows indicate the direction of EMT.

Based on the Hovmöller diagram, EMT shows a consistent pattern of strengthening in the east and weakening in the west, with very low intensity in the Sawu Sea region.

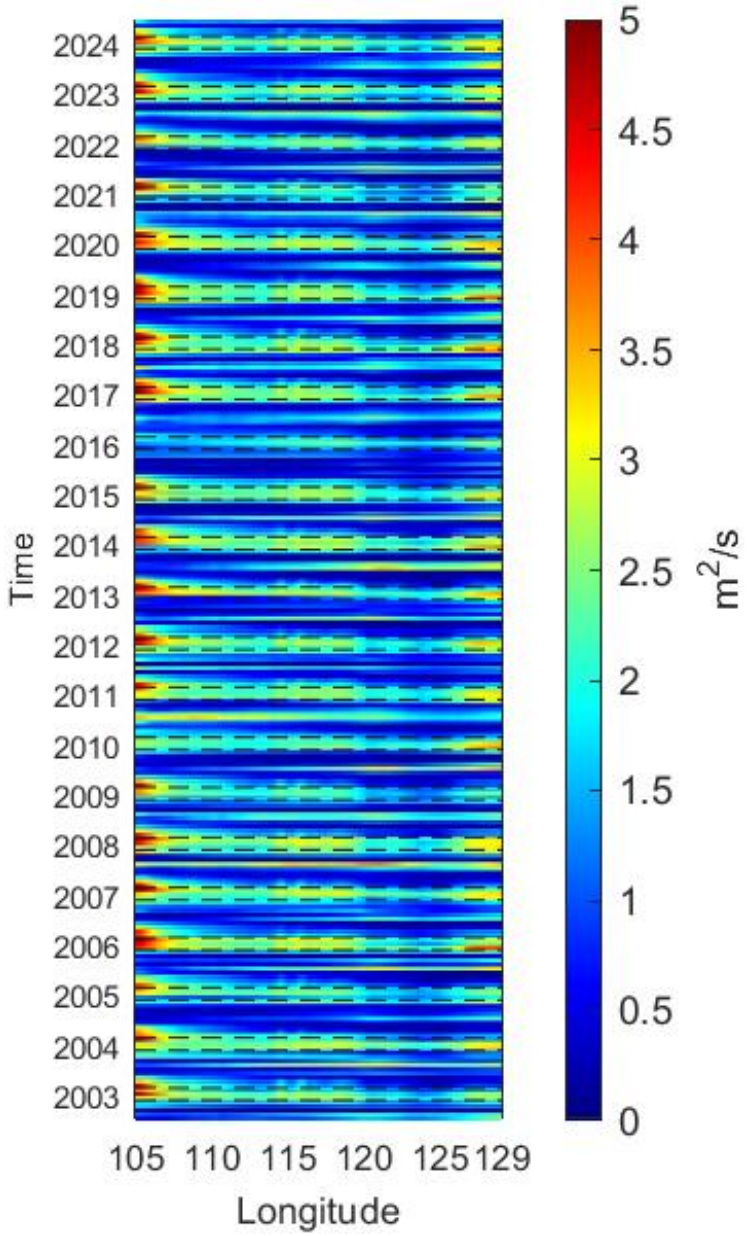


**Figure 4.** The Hovmöller diagram depicts the longitudinal-temporal variability of EMT. The EMT phenomenon is more varied during the JJA season, as indicated by the dotted line.

Table 3, comparing EMT values by region (marked on the research map) and season, shows that region D has the lowest values, while region A has the highest during the Southeast monsoon.

**Table 3.** Comparison of seasonal average values of EMT in regions A-D.

| Season / Region | Southeast Monsoon (DJF) | Transition Season I (MAM) | Northwest Monsoon (JJA) | Transition Season II (SON) |
|---|---|---|---|---|
| A | 0.67143646 | 1.223552151 | 3.104503656 | 2.493846008 |
| B | 1.139267844 | 1.172083539 | 2.710380049 | 1.259577608 |
| C | 1.124992309 | 1.171346478 | 2.818642489 | 1.12742054 |
| D | 0.409728264 | 0.238223529 | 0.52742304 | 0.292968493 |

Figure 4 shows the Hovmöller EMT diagram, with dotted lines indicating the JJA coverage limits for each year. Based on Figures 3 and 4, the Sawu Sea to the Ombai Strait shows a low EMT value. Table 3 shows that region D has the lowest EMT value. This may occur because the ITF transports Pacific water masses to the Indian Ocean, thereby reducing the surface water divergence required to trigger offshore EMT [45]. Additionally, high EMT patterns occur south of Java, across East Nusa Tenggara, and in the Wetar Strait, where surface sea cooling increases the thermohaline gradient. According to [27]This could potentially strengthen coastal currents and accelerate the transport of water masses from the Pacific Ocean to the Indian Ocean via the ITF. The diagram shows that EMT values were lower in 2010 and 2016 than in other years. The decrease in EMT values in 2010 (2016) compared to normal years is attributed to La Niña and the negative IOD (negative IOD) [14] [28].

**Variability Ekman Pumping Velocity**

Figure 5 shows the monthly average EPV, where positive and negative values mean downwelling and upwelling EPVs, respectively. January and February exhibit downwelling EPV along the southern coast of Java and the Sawu Sea. The Coriolis force causes ocean currents to trend to the left of the wind direction, resulting in a buildup of surface seawater that then descends to the lower layers [29]. From April to November, upwelling EPV dominates due to the influence of the Southeast monsoon. Monthly variations in EPV indicate changes in the dominance of upwelling and downwelling processes throughout the annual cycle. The spatial pattern of EPV shows differences in intensity between coastal and offshore areas. Each season shows differences in EPV, with gradual changes.

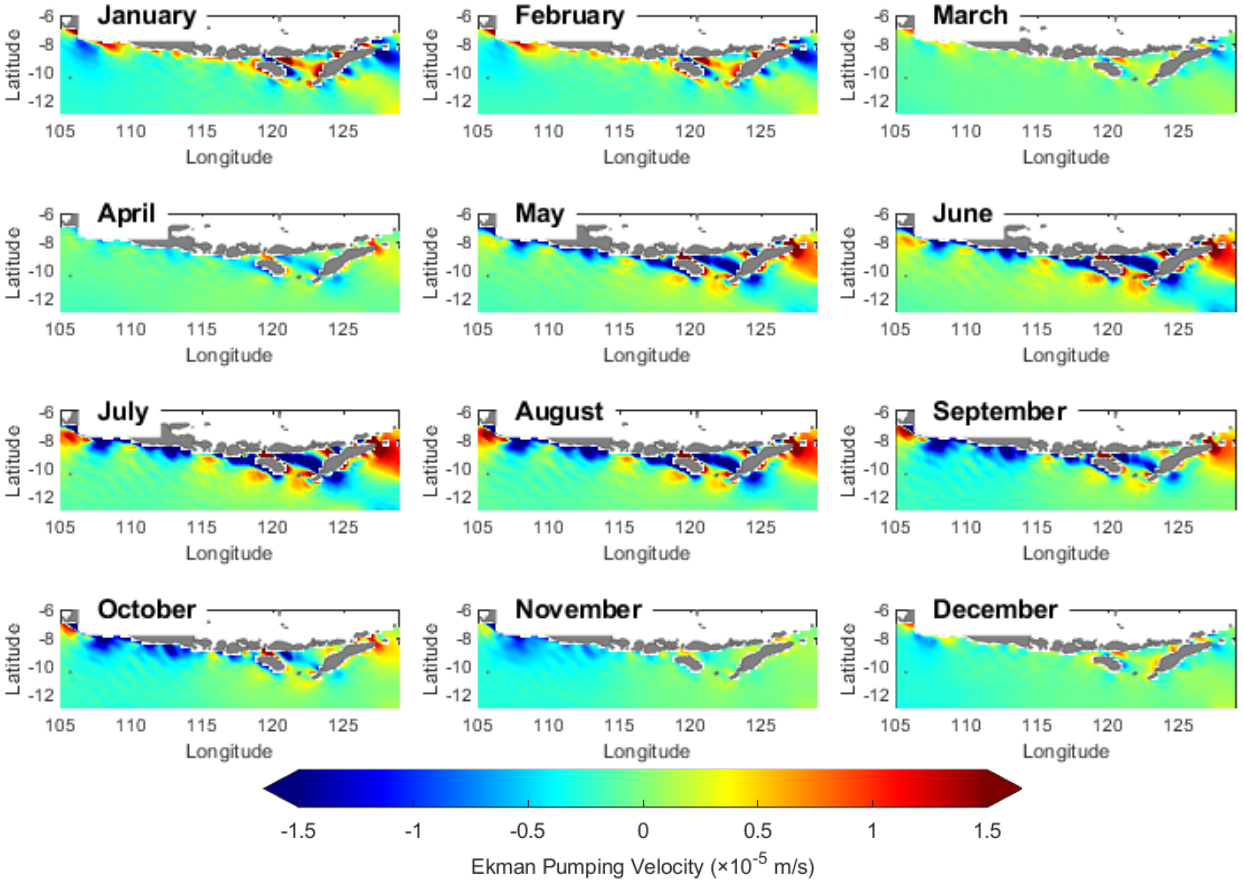


**Figure 5.** Monthly variability of EPV, negative values indicate upwelling, while positive values indicate downwelling.

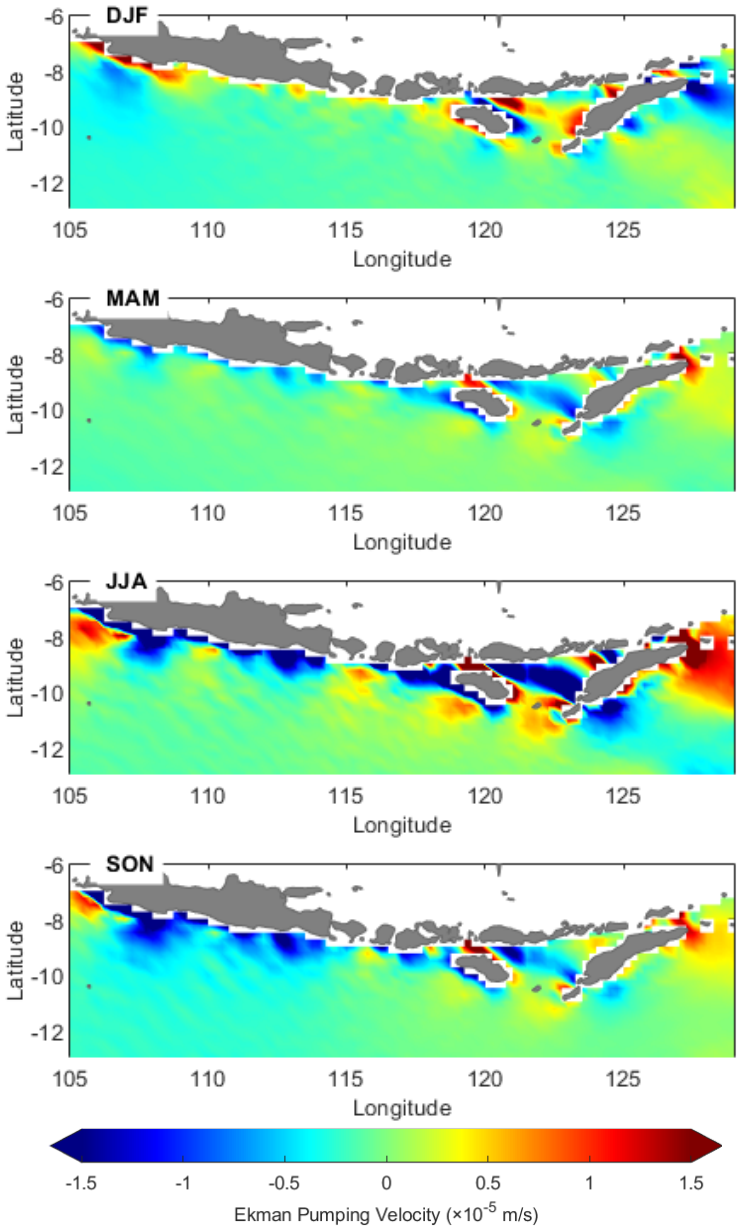


**Figure 6.** Seasonal variability of EPV, negative values indicate upwelling, while positive values indicate downwelling.

Consistent seasonal patterns show that EPV strengthens in the east and weakens in the west each year.

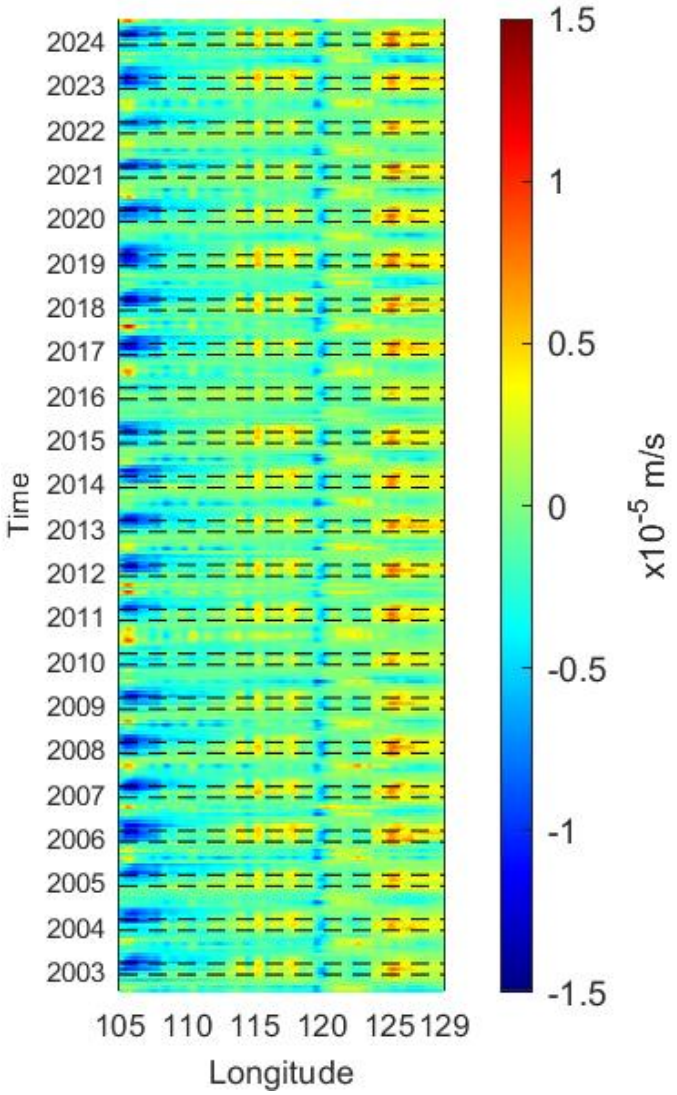


**Figure 7.** The Hovmöller diagram depicts the longitudinal-temporal variability of EPV The EPV phenomenon is more varied in the JJA season, which is marked with a dotted line.

Table 4 shows that region D has the highest negative EPV (upwelling) during the Southeast Monsoon season. Meanwhile, the region with the most positive EPV (downwelling) is region C.

**Table 4.** Comparison of seasonal average values of EPV in regions A-D.

| Season / Region | Southeast Monsoon (DJF) | Transition Season I (MAM) | Northwest Monsoon (JJA) | Transition Season II (SON) |
|---|---|---|---|---|
| A | -0.283243507 | -0.112161768 | -0.081841432 | -0.245730736 |
| B | -0.108702923 | -0.074063905 | -0.124134912 | -0.343963488 |
| C | -0.073890675 | 0.027141876 | 0.245922856 | -0.073769706 |
| D | -0.039332106 | -0.295240796 | -0.811252479 | -0.449970086 |

Figure 6 shows seasonal averages, with EPV values varying but very low in offshore areas. The Southeast Monsoon (DJF) has a negative value reaching -1.97 x $10^{-5}$ m/s in the eastern area of the Southern Java Sea and Sawu Sea, while around the Timor Sea, it has positive values reaching 2.39 x $10^{-5}$ m/s. In the Transition Monsoon I (MAM), the EPV is negative, reaching -1.43 x $10^{-5}$ m/s in the area of the southern Java Sea and the Sawu Sea, while around the Timor Sea it reaches 1.82 x $10^{-5}$ m/s. During the Northeast Monsoon (JJA), the onshore region from southern Java to the Sawu Sea has a negative EPV reaching -2.89 × $10^{-5}$ m/s, while the eastern region has a positive EPV reaching 2.44 × $10^{-5}$ m/s. Meanwhile, during the transition season II (SON), EPV begins to weaken. This pattern also corresponds with Table 4, which shows that EPVs in regions A-D are generally negative during the Southeast Monsoon (DJF) and Transition II (SON) seasons, in line with the dominance of downwelling in the southern coastal region of Java to the Sawu Sea. Meanwhile, in region C during the Northeast Monsoon (JJA) season, EPV strengthens in the eastern part of the study area. This study's results align with those of studies that are consistent with the research by [2] and [4]. EPV values tend to vary between the Southeast and Northwest Monsoons, depending on the region. Strong EPV values during the Southeast Monsoon occur due to east seasonal winds, leading to upwelling [30]. However, the strong upwelling occurred in the coastal areas and weakened when it reached the Indian Ocean [31]. Additionally, EPV is greatly influenced by wind curl, which is strongest near the coast, and coastal topography forms a strong wind curl gradient [2]. According to [32], coastal areas or areas along the equator are the widest and longest areas for water mass divergence.

Figure 7 shows a Hovmöller diagram depicting the annual cycle in the extraction area, with anomalies in EPV observed in 2010 and 2016. The EPV anomalies in 2010 (2016) compared to normal years occurred due to the La Niña and negative IOD (negative IOD) [14], [28] . During La Niña, the decrease in monsoon wind speed results in reduced upwelling intensity [11]. While this diagram confirms a consistent annual pattern, it also highlights correlations with the global climate phenomena.

### Correlation Between EMT and EPV with SST Anomalies and Chlorophyll-a Anomalies

Figure 8 (A) shows the distribution of correlations between SST anomalies and EMT over 22 years, with an average value of -0.13 in the eastern part of research area. Additionally, the positively correlated region (red) has an average of 0.15 and a maximum value of 0.35 on the southern coast of Java, indicating a low relationship. Meanwhile, the monthly correlation graph between SST and EMT (Figure 9) shows that negative correlations dominate, indicating an inverse relationship

between the two variables. In the study by [14] on the south coast of the Lesser Sunda Islands, the correlation ranges from -0.5 to -0.61, indicating a moderate negative correlation. Meanwhile, the study by [2] in Southern Java reported a moderate positive correlation of 0.49-0.53. This difference is likely due to the fact that those studies used data spanning 14 years (2007–2020) and 12 years (2007–2018), respectively, while this study used data spanning 22 years. Therefore, it covers more ENSO and IOD phenomena, leading to differences in correlation analysis results. EMT can cause changes in SST through divergence, which produces negative SST anomalies, or convergence of water masses, which produces positive SST anomalies on the sea surface [33]. This is consistent with the research by [34], which states that onshore EMT can increase positive SST anomalies, meaning a positive correlation.

Figure 8 (B) shows the correlation value of SST anomalies with EPV for 22 years. The results show that the negative correlation (blue) has an average of -0.15 in onshore South Java, offshore Nusa Tenggara, and the eastern part of the study area. Meanwhile, the region with a positive correlation (red) has an average of 0.15, which includes South Central Java to Bali and the Timor Sea. EPV can influence SST through upwelling and downwelling processes. However, Figure 10. shows the monthly correlation between EMT and chlorophyll a for the four regions plotted. Regions A, B, and D show predominantly positive values. According to [2], Southern West Java is characterized by downwelling EPV, while Southern East Java tends to experience more upwelling EPV. This demonstrates the inconsistency between SST and wind speed during the Southeast monsoon season and its relationship to wind stress curl. Positive correlations indicate that an increase in negative EPV (upwelling) is associated with a decrease in SST, while EPV downwelling is associated with an increase in SST. Region C shows a dominant negative value, indicating that the two variables have opposing values. The correlation between SST anomalies and EPV reflects the relationship between the vertical movement of seawater mass influenced by wind forces. One example is that strong Northeast Monsoon winds tend to produce EPV upwelling by strengthening wind stress curl [2].

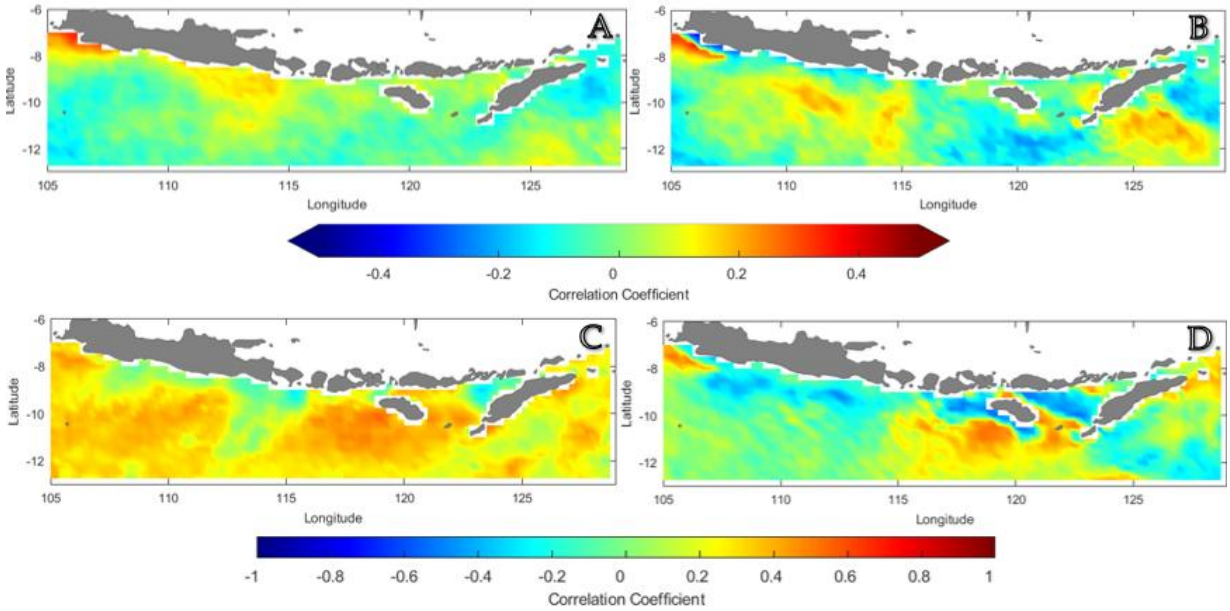


**Figure 8**. (A) Correlation Between SST Anomalies And EMT, (B) Correlation Between SST Anomalies And EPV, (C) Correlation Between Chlorophyll-A Anomalies And EMT, (D) Correlation Between Chlorophyll-A Anomalies And EPV.

Additionally, according to [35], decreases in SST are generally caused by vertical mixing. Similarly, the correlation between SST anomalies and EMT was fairly low because this study spanned 22 years and included many anomalies.

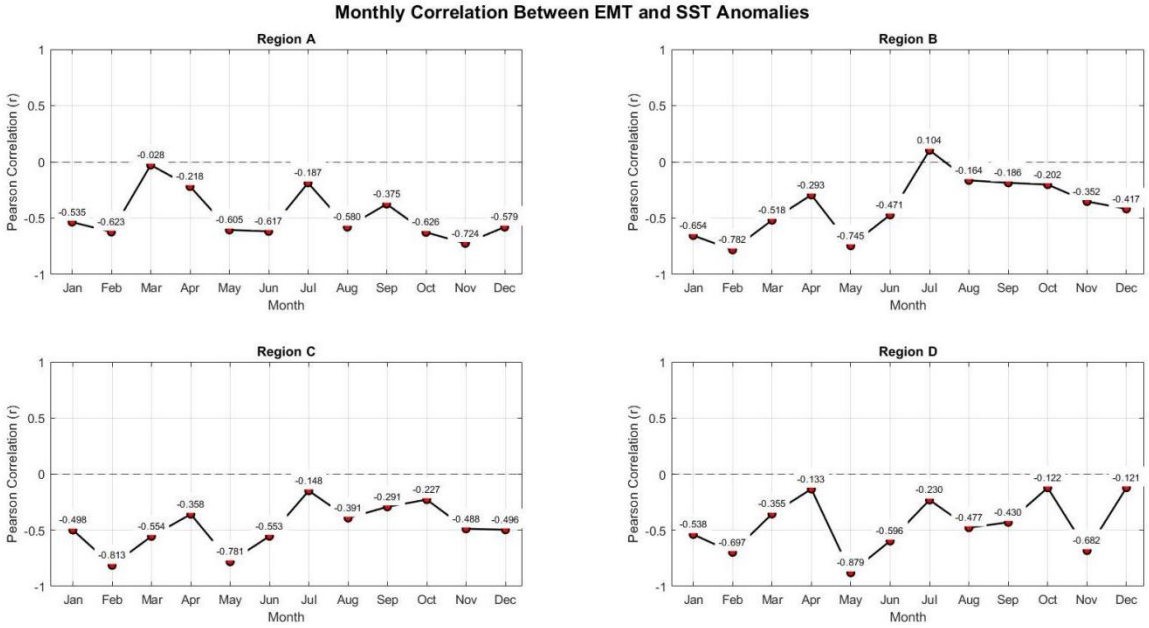


**Figure 9.** Monthly correlation of EMT and SST anomalies (2003–2024) in four subregions of the study area: region A (southwest of Java), region B (southeast of Java), region C (south of Bali), and region D (the Sawu Sea)

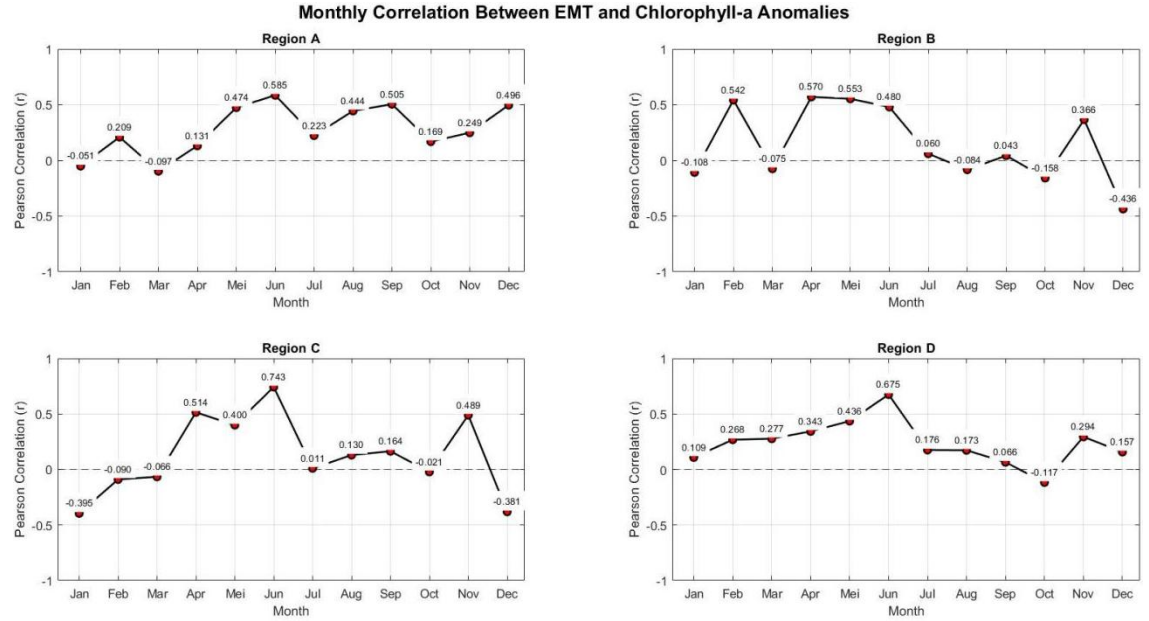


**Figure 10.** Monthly correlation of EMT and Chlorophyll-a anomalies (2003–2024) in four subregions of the study area: region A (southwest of Java), region B (southeast of Java), region C (south of Bali), and region D (the Sawu Sea).

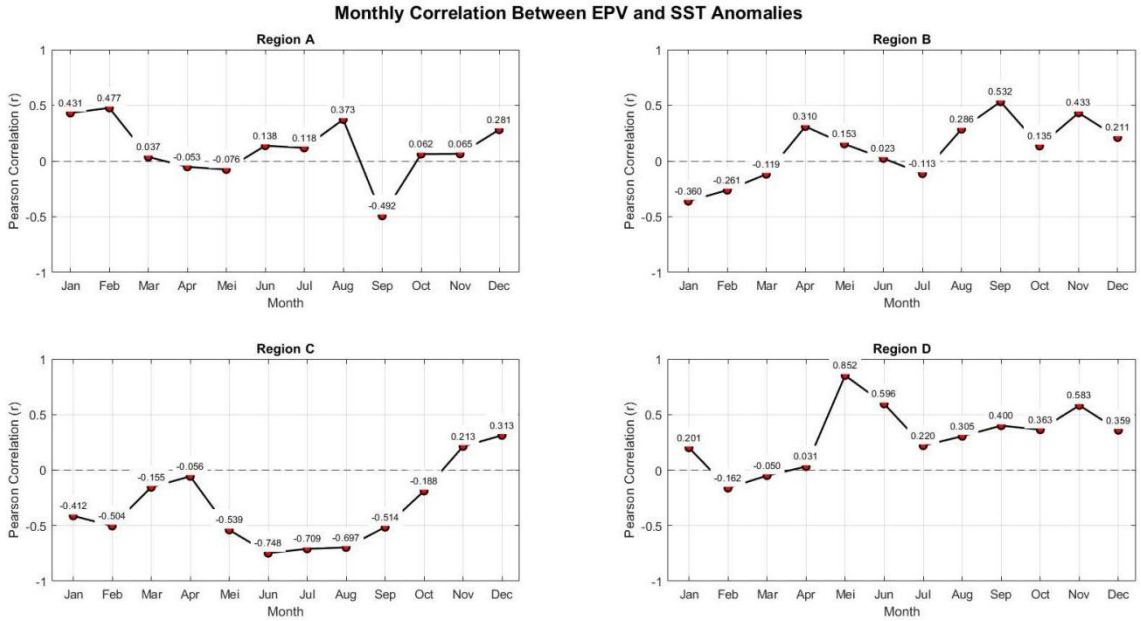


**Figure 11.** Monthly correlation of EPV and SST anomalies (2003–2024) in four subregions of the study area: region A (southwest of Java), region B (southeast of Java), region C (south of Bali), and region D (the Sawu Sea).

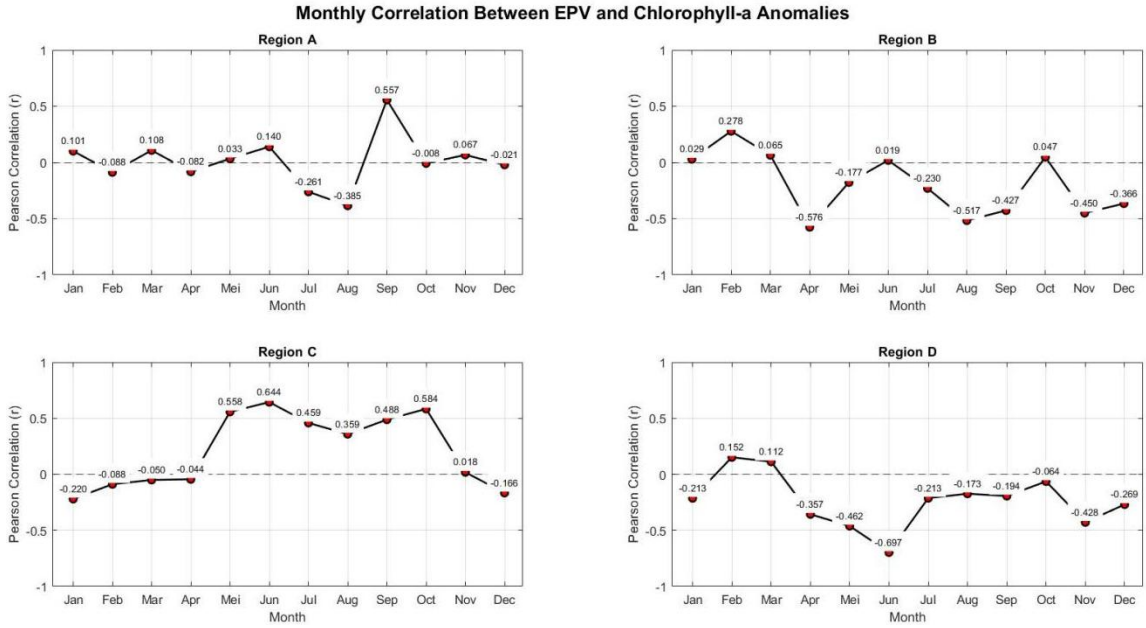


**Figure 12.** Monthly correlation of EPV and Chlorophyll-a anomalies (2003–2024) in four subregions of the study area: region A (southwest of Java), region B (southeast of Java), region C (south of Bali), and region D (the Sawu Sea).

The correlation between chlorophyll-a anomalies and EMT (Figure 8(c)) shows a positive correlation with an average of 0.32, indicating a low correlation; the highest value is 0.55. However, the value with a negative correlation is -0.17, which is very low. This correlation is fairly widespread in offshore areas. The monthly correlation graph between EPV and SST anomalies (Figure 11) also shows a more dominant positive correlation. This indicates a direct relationship, as EMT values increase, chlorophyll-a concentration also increases. According to

[36], the distribution of chlorophyll-a concentrations in offshore can be influenced by EMT because it reflects the horizontal transport capacity of seawater, which is driven by onshore wind stress. This indicates that EMT plays a role in increasing chlorophyll-a concentrations by triggering an upwelling mechanism that transports nutrients from depths to the surface layer of the ocean [34]. Some areas showing negative correlations may indicate other factors contributing to chlorophyll-a anomalies in onshore areas, one of which is EPV.

The correlation between chlorophyll-a anomalies and EPV (Figure 8 (d)) reflects the relationship between vertical dynamics and primary productivity. Positive values averaged 0.32 and reached a maximum of 0.53, dominant in the eastern region, indicate that negative EPV increases (upwelling) contribute to increased primary productivity through higher chlorophyll-a concentrations. This aligns with the theory that upwelling can bring nutrients from depth to the surface, enhancing phytoplankton growth and increasing chlorophyll-a concentrations [36]. The deeper layers are rich in nutrients and contain cold water masses [31]. Additionally, there are negative correlation values in some onshore locations that are dominant in the western region. According to [2], when the easterly wind is strong, wind stress curl tends to produce positive EPV (downwelling), thereby inhibiting onshore upwelling in the western region. The monthly correlation graph (Figure 12) also shows distinct correlation patterns across regions: regions A and C exhibit predominantly positive values, while regions B and D exhibit predominantly negative values. The varying correlation patterns across regions indicate that the relationship between EPV and chlorophyll-a concentration is strongly influenced by local oceanographic dynamics, seasonal variations, and surface current characteristics. Additionally, the simultaneous presence of positive and negative correlations can reduce the magnitude of the correlation. This is supported by the statistical principle that heterogeneous data can influence the average correlation value [37].

**Correlation Between EMT and EPV with ENSO and IOD**

Figure 13 (A) shows the distribution of correlation values between EMT and ENSO, which are very low and have an average of -0.03. This study shows that the ENSO phenomenon has a very limited effect on EMT in the study area. Based on the research by [38] in the Southern Java Sea, it was found that EMT is more influenced by other factors such as seasonal variability and the IOD phenomenon. Partial and non-partial analyses by [7] further support that the contribution of ENSO to EMT is lower compared to IOD. Meanwhile, Kelvin waves, which are long-range forces, can also cause upwelling by bringing nutrient-rich water masses towards the surface and putting it into the mixed layer [39]. Therefore, although ENSO is a global climate phenomenon with significant impacts in some regions, it does not have a statistically significant impact on EMT. The monthly correlation graph for the four regions (Figure 14) shows a similar pattern. The period from January to February shows a moderate negative correlation, while November shows a fairly high positive correlation. In the middle of the year, the relationship between EMT and ENSO weakens, possibly due to local variability or interaction with other climate phenomena. According to [40], La Nina can weaken the EMT by causing a weakening of the southern winds, especially when it occurs simultaneously with a negative IOD. One such was in 2010, when both the negative IOD and La Nina occurred. In other waters, offshore EMT weakened during La Nina and negative IOD in the Lesser Sunda Islands [41].

The correlation between EMT and IOD (Figure 13 (B)) shows a positive correlation, with an average of 0.14 (very low) and a maximum of 0.298 (low). Additionally, the monthly correlation graph between EMT and IOD (Figure 15) in the plotted area shows a predominantly positive relationship. However, the monthly correlation is highly fluctuating in the Sawu Sea, possibly triggered by the ITF flow from Banda Sea and the movement of the SJCC towards the Ombai Strait. According to [48], research in the offshore central Maluku Islands indicates that the positive correlation between IOD and EMT results in phytoplankton growth and a cooling of SST. The waters south of Java indicate that the EMT is more influenced by seasonal variability and IOD phenomena [38]. Furthermore, based on research by [42], Kelvin waves moving eastward along the equator to the west coast of Sumatra and Rossby waves moving westward from the Nusa Tenggara waters to the west coast of Sumatra can impact EMT. Therefore, the correlation between EMT and IOD is more evident only during periods of extreme IOD.

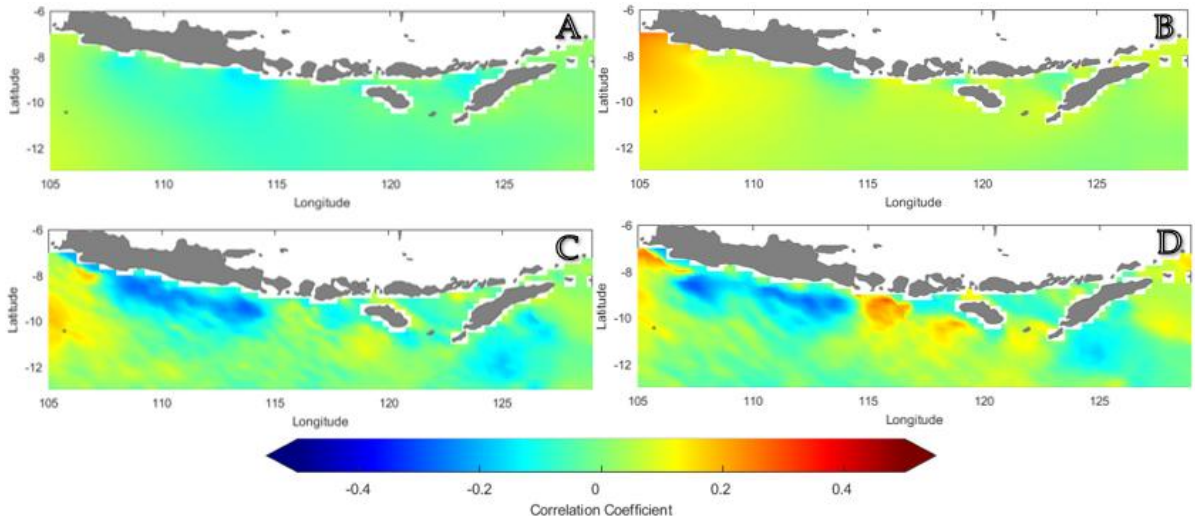


**Figure 13**. (A) Correlation Between EMT And ENSO, (B) Correlation Between EMT And IOD, (C) Correlation Between EPV And ENSO, (D) Correlation Between EPV And IOD

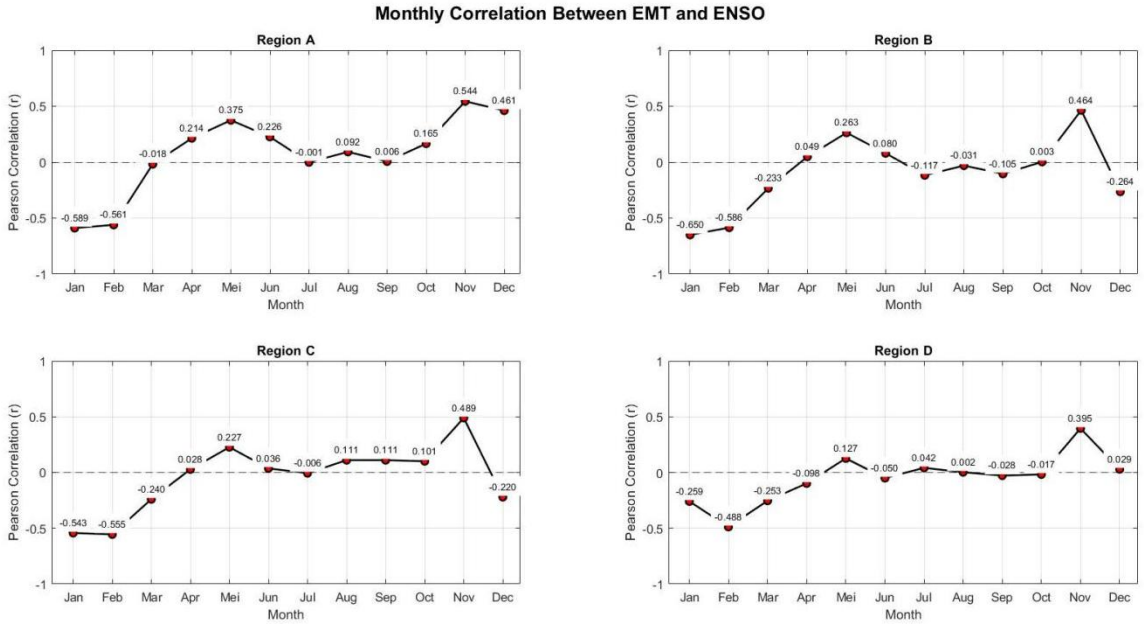


**Figure 14.** Monthly correlation between EMT and ENSO (2003–2024) in four subregions of the study area: region A (southwest of Java), region B (southeast of Java), region C (south of Bali), and region D (the Sawu Sea).

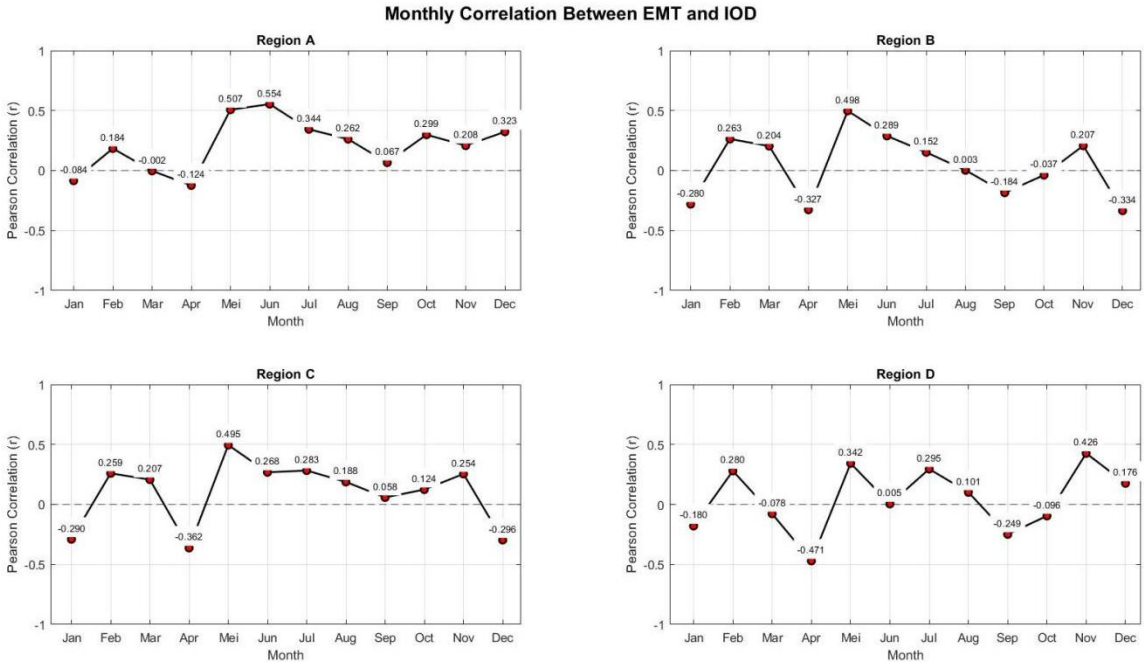


**Figure 15.** Monthly correlation between EMT and IOD (2003–2024) in four subregions of the study area: region A (southwest of Java), region B (southeast of Java), region C (south of Bali), and region D (the Sawu Sea).

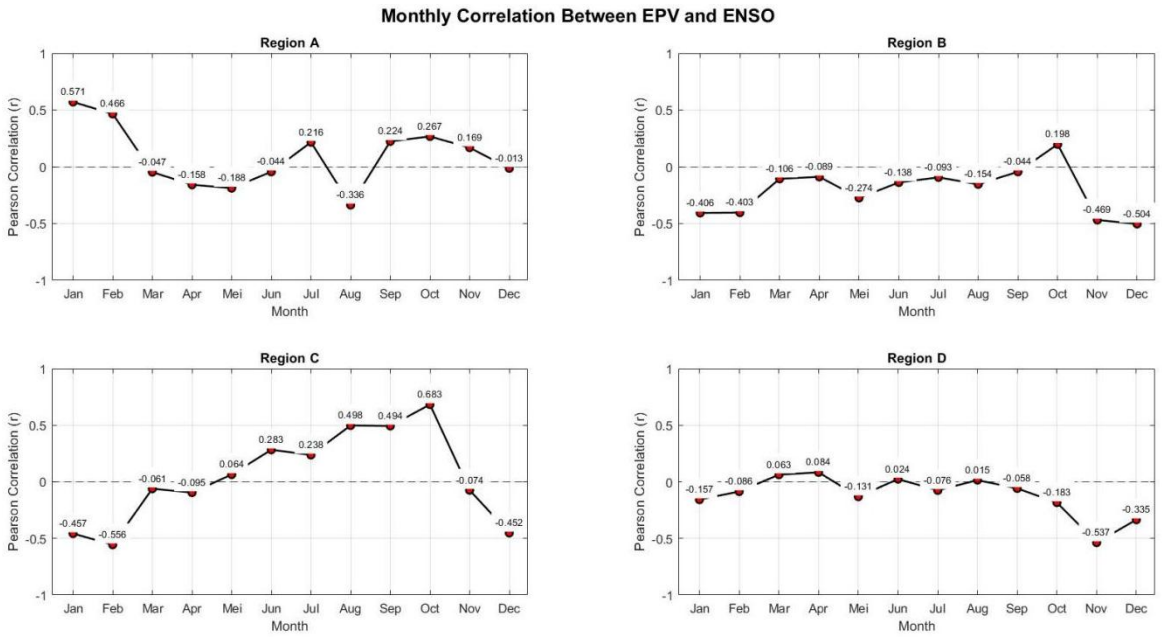


**Figure 16.** Monthly correlation between EPV and ENSO (2003–2024) in four subregions of the study area: region A (southwest of Java), region B (southeast of Java), region C (south of Bali), and region D (the Sawu Sea).

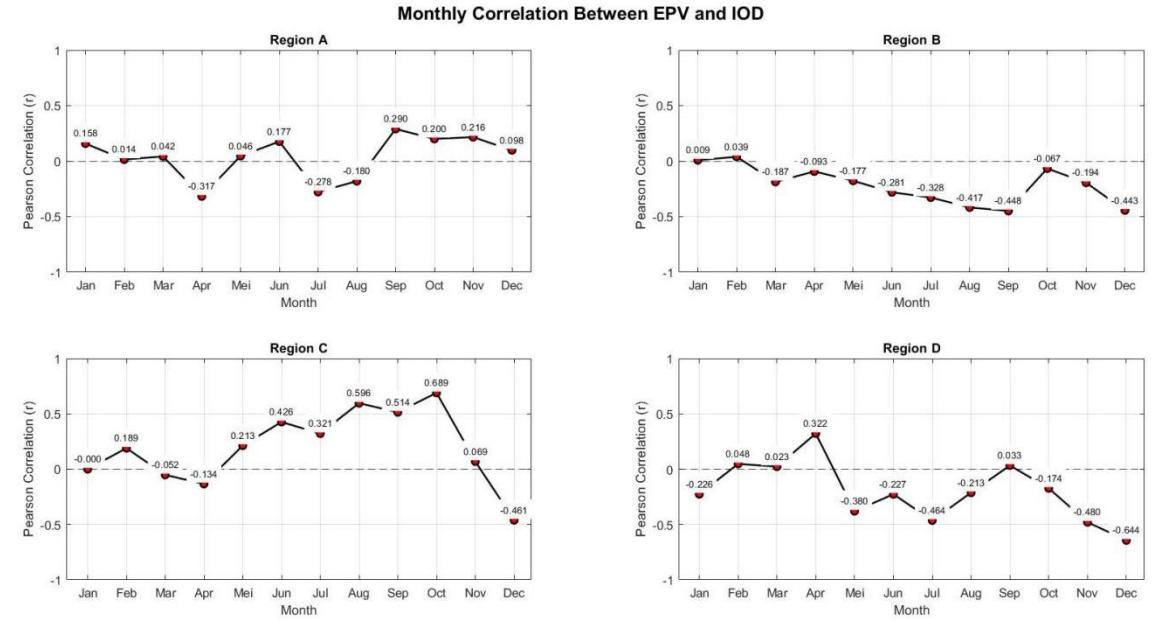


**Figure 17.** Monthly correlation of EPV and IOD (2003–2024) in four subregions of the study area: region A (southwest of Java), region B (southeast of Java), region C (south of Bali), and region D (the Sawu Sea).

The correlation between EPV and ENSO (Figure 13(C)) is very low, with an average of 0.13 and a maximum of 0.19. The very low positive correlation may be due to changes in wind direction or to interactions with the IOD. A very low positive correlation indicates that EPV is influenced by the La Niña phase, during which trade winds tend to be stronger and can increase upwelling in some regions. In the waters south of Java and West Nusa Tenggara, there tends to be a negative correlation, indicating that ENSO in the El Niño phase decreases EPV

values, weakening upwelling activity. Based on the research by [38], the 2010 La Niña phase showed stronger upwelling, while in the 2015 El Niño phase, the thermocline layer became deeper, so that the water mass rising to the surface was warmer and less nutrient-rich, thereby weakening water productivity. The weak correlation in some other regions indicates that other factors have a greater influence on EPV. The monthly correlation graph between EPV and ENSO (Figure 16) shows distinct patterns: Region C shows relatively high values, while Region D shows lower values. The region exhibits a consistently increasing correlation, peaking in October. According to [43], the increase in this correlation indicates the dominance of ENSO signals over physical dynamics south of Bali.

The correlation between EPV and IOD (Figure 13(d)) is positive across southern western Java and Bali to East Nusa Tenggara, consistent with the monthly correlation graph (Figure 17). This indicates that a positive correlation means positive IOD values are associated with an increase in negative EPV (upwelling). Meanwhile, the region with the lowest negative correlation is central eastern Java, suggesting that negative IOD can be associated with positive EPV (downwelling). This aligns with the research by [14], which found that in 2016, negative IOD occurred, indicating downward water movement (downwelling). Meanwhile, during the positive IOD in 2008, a negative SST anomaly and positive chlorophyll-a anomaly occurred, indicating upwelling. Additionally, based on the research by [44] and [2], a positive IOD triggers greater upwelling than ENSO.

The interaction between ENSO and IOD is a crucial factor in the dynamics of the tropical atmosphere and oceans, significantly impacting the EMT and EPV. This phenomenon can weaken or alter the direction of EMT, strengthen or weaken EPV, and affect regional ocean circulation. The interaction between ENSO and IOD significantly influences EMT, potentially weakening or altering its direction and affecting regional ocean circulation. For instance, in [2], which found that the combination of La Niña and negative IOD can weaken the offshore EMT and reduce chlorophyll-a concentrations and SST cooling during the southeast monsoon season. Meanwhile, positive EPV indicates the presence of downwelling offshore, particularly in the waters off the south coast of Bali to Sumbawa [14]. However, in the study by [7], which used a partial correlation between ENSO and IOD with upwelling, shows that ENSO's influence occurs in November in the western region, even after IOD's influence is removed in the Southern Indonesian Waters. The IOD phenomenon is more influential because the study area faces the Indian Ocean [42].

## Conclusion

During the Southeast Monsoon (JJA), EMT (EPV) is stronger compared to other seasons, with a range of values reaching up to 5.16 $m^2/s$ ($-2.89 \times 10^{-5}$ m/s). Spatially, Region A exhibited the highest EMT, while Region D showed the highest EPV (upwelling). The dominant phenomenon in this study area is EMT, as it occurs at the sea surface. In 2010 and 2016, the combination of La Niña and a negative IOD resulted in significantly lower EMT and EPV values compared to other years. Correlation analysis of EMT and EPV with SST and chlorophyll-a shows that, in offshore areas, SST is more influenced by EPV than by EMT. Conversely, chlorophyll-a is more influenced by EMT, with increased concentrations observed in offshore zones. Overall, EMT and EPV are more strongly influenced by the IOD than by ENSO due to the region's geographical location facing the Indian Ocean.

## References


[1] E. Aldrian, *Meteorologi Laut Indonesia*, no. June 2008. 2008.

[2] A. Wirasatriya *et al.*, "Ekman dynamics variability along the southern coast of Java revealed by satellite data," *International Journal of Remote Sensing*, vol. 41, no. 21, pp. 8475–8496, 2020.

[3] D. Wang, H. Wang, M. Li, G. Liu, and X. Wu, "Role of Ekman transport versus Ekman pumping in driving summer upwelling in the South China Sea," *Journal of Ocean University of China*, vol. 12, no. 3, pp. 355–365, 2013.

[4] E. M. J. Putri and J. Wirasatriya, Anindya, Marwoto, "Pengaruh Ekman Mass Transport dan Ekman Pumping Velocity Terhadap Upwelling di Perairan Selatan Pulau Bali-Sumbawa," vol. 05, no. 03, pp. 118–130, 2023.

[5] H. I. Ratnawati, R. Hidayat, A. Bey, and T. June, "Upwelling di Laut Banda dan Pesisir Selatan Jawa serta Hubungannya dengan ENSO dan IOD," *Omni-Akuatika*, vol. 12, no. 3, pp. 119–130, 2016.

[6] D. Suman, A., Wudianto, Sumiono, B., Badrudin, Nugroho, D., Merta G. S., Suwarso, Taufik, M., Amri, K., Kembaren, *Potensi dan Tingkat Pemanfaatan Sumber Daya Ikan di Wilayah Pengelolaan Perikanan Republik Indonesia (WPP RI)*. Jakarta: Ref Graphika, 2014.

[7] H. A. Rachman *et al.*, "Dynamic of upwelling variability in southern Indonesia region revealed from satellite data: Role of ENSO and IOD," *Journal of Sea Research*, vol. 202, no. August, p. 102543, 2024.

[8] R. B. Yoga, H. Setyono, and G. Harsono, "Dinamika Upwelling Dan Downwelling Berdasarkan Variabilitas Suhu Permukaan Laut Dan Klorofil-a," *Oseanografi*, vol. 3, no. 1, pp. 57–66, 2014.

[9] I. N. A. Diputra, "Variability of SST, CHL-A, and Wind in the South Java – Nusa Tenggara Waters From 2003 – 2023 and Its Relation to ENSO and IOD Phenomena.," Udayana University, 2024.

[10] A. Kurnianingsih, T. N., Sasmito, B., Prasetyo, Y., & Wirasatriya, "Analisis sebaran suhu permukaan laut, klorofil-a, dan angin terhadap fenomena upwelling di perairan Pulau Buru dan Seram.," *Jurnal Geodesi Undip*, vol. 6(1), pp. 238–248, 2017.

[11] U. O. Nurafifah, M. Zainuri, and A. Wirasatriya, "Pengaruh ENSO dan IOD Terhadap Distribusi Suhu Permukaan Laut dan Klorofil-a Pada Periode Upwelling di Laut Banda," *Indonesian Journal of Oceanography*, vol. 4, no. 3, pp. 74–85, 2022.

[12] Q. Taufikurahman and R. ; Hidayat, "Coastal Upwelling in Southern Coast of Sumbawa Island, Indonesia," in *Journal of Physics: Conference Series*, 2016.

[13] S. Ginanjar, M. F. Syach, and S. Wulandari, "Kajian pengaruh siklon tropis mangga terhadap curah hujan, transpor Ekman, viskositas Eddy dan tinggi gelombang di perairan selatan Jawa pada 20-25 Mei 2020," *Jurnal Meteorologi Klimatologi dan Geofisika*, vol. 7, no. 2, pp. 15–23, 2020.

[14] F. Simanjuntak and T. H. Lin, "Monsoon Effects on Chlorophyll-a, Sea Surface Temperature, and Ekman Dynamics Variability along the Southern Coast of Lesser Sunda Islands and Its Relation to ENSO and IOD Based on Satellite Observations," *Remote Sensing*, vol. 14, no. 7, 2022.

[15] Martono, "Seasonal and Interannual Variations of Sea Surface Temperature in the Indonesian Waters," vol. 30(2), pp. 120–129, 2016.

[16] A. Corredor-Acosta *et al.*, "Spatio-temporal variability of chlorophyll-a and environmental variables in the Panama bight," *Remote Sensing*, vol. 12, no. 13, 2020.

[17] ESRI, "Aggregate (spatial analyst) - ArcMap." Accessed: Jun. 15, 2025. [Online]. Available: https://desktop.arcgis.com/en/arcmap/latest/tools/spatial-analysttoolbox/aggregate.htm

[18] C. Candra and A. Sakban, "Analisis korelasi kepemimpinan kepala sekolah dan kinerja guru terhadap motivasi belajar siswa di SMAN 1 Labuapi Kabupaten Lombok Barat," *Jurnal Ilmiah Manda Education*, vol. 2(2), pp. 53–60, 2016.

[19] D. S. Graha, Kunarso, and M. Zainuri, "Variabilitas Antar Tahunan Suhu Permukaan Laut dan Klorofil-A Terhadap Hasil Tangkapan Ikan Kembung (Rastreligger Sp.) di Perairan Demak," *Indonesian Journal of Oceanography*, vol. 6, no. 2, pp. 148–158, 2024.

[20] J. E. V Siahaan, K. Kunarso, and Y. J. Wijaya, "Variasi Temporal Dinamika Upwelling di Selat Makassar Periode 2007-2021," *Buletin Oseanografi Marina*, vol. 13, no. 1, pp. 122–135, 2024.

[21] A. S. Budiman, D. G. Bengen, I. W. Nurjaya, Z. Arifin, and M. F. A. Ismail, "A Comparison of the Three Upwelling Indices in the South Java Sea Shelf," *Chiang Mai University Journal of Natural Sciences*, vol. 21, no. 3, 2022.

[22] W. J. Moses *et al.*, "Estimation of chlorophyll- a concentration in turbid productive waters using airborne hyperspectral data," *Water Research*, vol. 46, pp. 993–1004, 2011.

[23] J. D. Everett, M. E. Baird, M. Roughan, I. M. Suthers, and M. A. Doblin, "Progress in oceanography relative impact of seasonal and oceanographic drivers on surface chlorophyll-a along a western boundary current," *Progress in Oceanography*, vol. 120, pp. 340–351, 2014.

[24] H. Bernades *et al.*, "The effect of Ekman mass transport and Ekman pumping velocity on the variability of sea surface temperature in the Arafura Sea," in *IOP Conference Series: Earth and Environmental Science*, 2021.

[25] D. Oktaviani, G. Handoyo, M. Helmi, Kunarso, and A. Wirasatriya, "Karakteristik Upwelling pada Periode Indian Ocean Dipole (IOD) Positif di Perairan Selatan Jawa Barat," *Indonesian Journal of Oceanography*, vol. 3, no. 4, pp. 354–361, 2021.

[26] W. S. T. Pranowo *et al.*, *Sumber Daya NonHayati Maritim*, Seri Buku. Jakarta: Amafrad Press, 2019.

[27] J. Sprintall *et al.*, "The Indonesian seas and their role in the coupled ocean–climate system," *Nature Geoscience*, vol. 7, pp. 487–492, 2014.

[28] J. Lumban-Gaol *et al.*, "Impact of the strong downwelling (Upwelling) on small pelagic fish production during the 2016 (2019) negative (positive) indian ocean dipole events in the eastern indian ocean off java," *Climate*, vol. 9, no. 2, pp. 1–11, 2021.

[29] A. Syafik, Kunarso, and Hariadi, "Permukaan laut di Samudera Hindia (Wilayah Pengelolaan Perikanan Republik Indonesia 573)," *Jurnal Oseanografi*, vol. 2, no. 3, pp. 318–328, 2013.

[30] R. D. Susanto, Thomas. S. Moore, and J. Marra, "Ocean color variability in the Indonesian Seas during the SeaWiFS era," *Geochemistry, Geophysics, Geosystems*, vol. 7, no. 5, pp. 1–16, 2006.

[31] E. Mustikasari, L. C. Dewi, A. Heriati, and W. S. Pranowo, "Pemodelan pola arus barotropik musiman 3 dimensi (3D) untuk mensimulasikan fenomena upwelling di perairan Indonesia.," *Jurnal Segara*, vol. 11, no. 1, pp. 25–35, 2015.

[32] M. A. Wahid, "Kajian fenomena upwelling di perairan Sumatera bagian selatan serta mengidentifikasi pengaruhnya terhadap wilayah Aceh," Universitas Islam Negeri Ar-Raniry, 2023.

[33] D. Okgareta, I. Wayan Nurjaya, Y. Naulita, and Rastina, "Oceanographic characteristics of Lampung Bay and its relationship to the Indian Ocean Dipole (IOD) period 2013-2021," *BIO Web of Conferences*, vol. 106, pp. 0–10, 2024.

[34] N. Kurniawati, D. O. Lestari, Fauziyah, D. Setiabudidaya, and I. Iskandar, "Variation of thermodynamic layers over the South Coastal Java Region (SJCR) and their influences on nutrient abundance," *Journal of Physics: Conference Series*, vol. 1568, no. 1, 2020.

[35] Z. Ruan, B. Li, C. Yu, R. Ding, P. Bai, and Q. Wu, "The impact of tropical cyclone outer size on ocean surface responses," *Frontiers in Marine Science*, vol. 11, no. July, pp. 1–11, 2024.

[36] X. Fang, X. Zhang, X. Chen, and W. Yu, "The Impact of Ekman Pumping and Transport on Dosidicus gigas (Jumbo Flying Squid) Fishing Ground by Chinese Jiggers off the Coast of Peru," *Journal of Marine Science and Engineering*, vol. 13, no. 2, 2025.

[37] R. J. Janse *et al.*, "Conducting correlation analysis: Important limitations and pitfalls," *Clinical Kidney Journal*, vol. 14, no. 11, pp. 2332–2337, 2021.

[38] A. S. Atmadipoera, A. S. Jasmine, M. Purba, and A. R. T. D. Kuswardani, "Upwelling Characteristics in the Southern Java Waters During Strong La Nina 2010 and Super El Nino 2015," *Jurnal Ilmu dan Teknologi Kelautan Tropis*, vol. 12, no. 1, pp. 257–276, 2020.

[39] G. Chen, W. Han, Y. Li, D. Wang, and T. Shinoda, "Intraseasonal variability of upwelling in the equatorial Eastern Indian Ocean," *Journal of Geophysical Research: Oceans*, vol. 120, pp. 7598–7615, 2015.

[40] U. Setiawan, R. Y., A. Wirasatriya, S. L. Hernawan, and I. Iskandar, "Spatio-temporal Variability of Surface Chlorophyll-a in the Halmahera Sea and Its Relation to ENSO and the Indian Ocean Dipole," *International Journal of Remote Sensing*, vol. 41, no. 1, pp. 284–299, 2020.

[41] A. Setiawan, R. Y., E. Setyobudi, A. Wirasatriya, A. S. Muttaqin, and L. Maslukah, "The Influence of Seasonal and Interannual Variability on Surface Chlorophyll-a off the Western Lesser Sunda Islands," *IEEE Journal of Selected Topics in Applied Earth Observations and Remote Sensing*, vol. 12, no. 1, pp. 4191–4197, 2019.

[42] M. F. K. Almunawir, A. Wirasatriya, and R. Widiaratih, "Pengaruh Fenomena IOD Positif Kuat 2019 Terhadap Karakteristik Upwelling di Perairan Nusa Tengggara," *Indonesian Journal of Oceanography*, vol. 6, no. 1, pp. 72–83, 2024.

[43] N. P. Purba, W. S. Pranowo, A. B. Ndah, and P. Nanlohy, "Seasonal variability of temperature, salinity, and surface currents at 0° latitude section of Indonesia seas," *Regional Studies in Marine Science*, vol. 44, no. 101772, 2021.

[44] D. H. Kunarso, Ismunarti, A. Rifai, B. Munandar, A. Wirasatriya, and R. D. Susanto, "Effect of Extreme ENSO and IOD on the Variability of Chlorophyll-a and Sea Surface Temperature in the North and South of Central Java Province," *ILMU KELAUTAN: Indonesian Journal of Marine Sciences*, vol. 28, no. 1, pp. 1–11, 2023.

[45] M. A. Rahman, M. L. Syamsudin, M. U. K. Agung, and Sunarto, "Pengaruh Musim Terhadap Kondisi Oseanografi dalam Penentuan Daerah Penangkapan Ikan Cakalang (Katsuwonus pelamis) di Perairan Selatan Jawa Barat," *J. Perikan. dan Kelaut.*, vol. X, no. 1, pp. 92–102, 2019.

[46] A. Persson, "The Story of the Hovmöller Diagram: an (Almost) Eyewitness Account," *Bull. Am. Meteorol. Soc.*, vol. 98, no. 5, pp. 949–957, 2017.

[47] A. Hartoko, "Oseanografi dan Sumber Daya Perikanan Kelautan di Indonesia," UNDIP Press, 2010.

[48] R.Y. Setiawan, E. Setyobudi, A. Wirasatriya, A.S. Muttaqis, and L. Maslukah, "Seasonal and Interannual Coastal Wind Variability of the Central Maluku Islands Revealed by Satellite Oceanography," *Global Nest Journal*, vol. 24, no. 1, 37-43, 2022.